Probing the $1\,^2\Sigma_u^+$ cation state by low-energy dissociative ionization of Na_2

B. Delahunty, K. Black, and L. Hüwel
Physics Department, Wesleyan University, Middletown, Connecticut 06459-0155
(Received 10 February 1999)

We have measured highly resolved time-of-flight spectra and concomitant angular distributions of slow Na^+ ions produced by near-threshold dissociative ionization of Na_2. Using double-resonance excitation via the $A\,^1\Sigma_u^+$ state, Na_2 molecules are promoted to rotational levels $J=14$ or 16 and vibrational levels between $v=50$ and 69 of the $4\,^1\Sigma_g^+$ state. Then, a third photon—from the second of two tunable dye lasers employed—causes the transition into the double continuum associated with the $1\,^2\Sigma_u^+$ potential of the Na_2^+ cation. A detailed Monte Carlo simulation is employed to study the dynamics of this dissociative ionization process in detail. Based on this approach, we were able to subject recent calculations of this $1\,^2\Sigma_u^+$ potential to experimental scrutiny. We find our data to be compatible with a zero-energy crossing near 8.8 Å and a well depth of about 70 cm^{-1}, which agrees with most of the published calculations. Angular distributions for the vibrational level $v=60$ are also reproduced well using the same potential parameters and an anisotropy parameter $\beta=2$ modified by a semiclassical argument to account for parent molecule rotation. [S1050-2947(99)07708-2]

PACS number(s): 34.20.Cf, 33.80.Gj, 33.80.Rv

I. INTRODUCTION

Dissociative ionization of diatomic molecules provides an intriguing example of a three-body process: upon absorption of one or more photons, breakup occurs into an electron, a neutral atom, and an ion. Because of the large mass difference, it is not easy to treat the dynamics of electronic and nuclear motion in the exit channel in a unified, simultaneous manner. Only recently has such a theoretical description been accomplished [1]; good agreement was found with data relating to the competition between ionization and dissociation [2] and the predissociation of singlet gerade states [3] in H_2. In fact, dissociative ionization usually occurs in competition with other product channels such as predissociation or ionization without fragmentation and this aspect and a host of related questions have been addressed in several recent experimental and theoretical papers. For example, experimental studies of dissociative ionization of CO [4] and O_2 [5] focus on the competition between dissociation and ionization—in the latter case far (more than 10 eV) above the ionization threshold. With a maximum possible fragmentation energy of 0.56 eV, a study of the single color (193 nm) 3-photon dissociative ionization of H_2 via the *E,F* state [6] shifts the emphasis closer to threshold and provides, in particular, a detailed analysis of the proton angular distribution. At a similar maximum fragment energy, the femtosecond dynamics of dissociative ionization of NaI has been the study of some quantum-mechanical simulations [7]. Even closer to threshold, our laboratory has reported [8] on a systematic investigation of dissociative ionization of Na_2 in vibrational levels from $v=50$ to 69 in the $4\,^1\Sigma_g^+$ state. For the lowest observed vibrational level, the maximum available center-of-mass fragmentation energy is only about 0.04 eV. Furthermore, for $v=52$ and 55, strong evidence exists for significant production of ion fragments with *zero* kinetic energy. The current paper expands on the discussion of these experimental results. Most importantly, we have reanalyzed how the time-of-flight (TOF) line shapes are influenced by the lowest ungerade state of the Na_2^+ molecular ion, the $1\,^2\Sigma_u^+$ potential, in particular, by its shape near the zero-energy crossing point and the depth of its shallow well. Core extraction and low-field mode operation of the TOF spectrometer allow for very efficient detection of slow fragments. Hence, our experiment is very sensitive to the near-threshold region and to the zero-energy crossing point of the—nominally repulsive—upper molecular potential and we exploit this sensitivity to test which of several recent calculations [9–15] best reproduces our results. Figure 1 shows the potential calculations for the ranges of internuclear distance and energy relevant to our experiment. As can be seen the various theoretical approaches agree very well. Nevertheless, small differences exist and our experimental data can reject at least one of these calculations. In order to use the *ab initio* points of the calculations for our purposes and also in order to better compare the different references to each other, we decided to use a six-parameter analytical expression as a fitting form to all published data [see Sec. IV, Eq. (5) and also

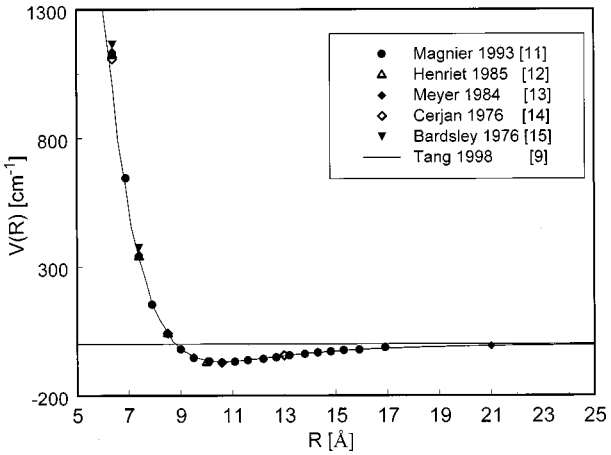

FIG. 1. Potential-energy curve of the $1\,^2\Sigma_d^+$ state of Na_2^+ according to six different calculations. The solid line is an analytical expression valid for the asymptotic region of exchange and dispersion interactions.

TABLE I. Parameter values in atomic units, zero-energy crossing point in Å, and well depth in cm^{-1} for best fits of the analytical potential function, Eq. (2), to recent calculations of the $1\,^2\Sigma_u^+$ potential.

Reference	A (a.u.)	β (a.u.)	α_1 (10^2 a.u.)	α_2 (10^3 a.u.)	α_3 (10^5 a.u.)	$-B$ (10^4 a.u.)	R_0 (Å)	V_{min} (cm^{-1})
[9]	0.768	0.614 59	1.592	1.86	0.55	6.1	8.83	67.8
[10]	0.579	0.612 39	1.905	−14.3	2.9	−4.0	8.43	74.3
[11]	0.741	0.616 09	1.653	1.13	−8.1	2.3	8.78	69.5
[12]	0.752	0.617 20	1.657	0.52	−7.0	2.4	8.78	69.6
[13]	0.776	0.618 74	1.606	2.42	−7.3	2.8	8.79	68.9
[14]	0.774	0.616 51	1.675	2.17	−5.0	3.7	8.77	72.0
[15]	0.771	0.615 02	1.701	0.95	−3.8	3.6	8.86	70.0

Table I]. The solid line shown in Fig. 1 represents this analytical expression with the parameter values from the original article [9]. We have also measured the polarization dependence of the TOF spectra for vibrational level 60 in the shelf state. Section III summarizes all our observations while Sec. IV presents a detailed discussion of the Monte Carlo simulation used to analyze our data. Section V explains the findings and how the observed TOF patterns can be accounted for. Experimental details of our work are provided in the following section.

II. EXPERIMENT

Apparatus. We have used a molecular beam apparatus in conjunction with a linear time-of-flight spectrometer of the Wiley-McLaren type [16], two pulsed, narrow-band dye lasers pumped by a single neodymium-doped yttrium aluminum garnet (Nd:YAG) laser, and a computer-controlled 100-MHz transient digitizer. With this set of instruments we can control input parameters and measure TOF spectra with the precision necessary for the experiments and analysis described in this paper. While pertinent aspects of the experimental setup can be found elsewhere [8,17,18], the subsequent description provides additional details of molecular beam, laser, and TOF spectrometer, some of which are also included in our simulation program.

The double-chamber beam source is heated by stainless steel sheathed nickel wires to temperatures of about 790 K and 720 K for nozzle and reservoir compartment, respectively. The resulting sodium vapor pressure in the reservoir is estimated to be about 5 to 10 torr. Under these operating conditions and with a nozzle diameter of approximately 0.5 mm, we expect a mild supersonic expansion. In an attempt to measure the Na_2 speed distribution in the beam, we have monitored the variation of the Na_2^+ TOF signal when polarity and strength of an electric field in the drift region of the TOF spectrometer (produced by a suitable pair of ''steering plates'') are changed systematically. Oriented parallel to the beam motion, this steering field allows a given speed range of Na_2^+ ions to reach the detector. From a careful analysis of such data we conclude that the molecular beam has a speed ratio of $S=3$ and a most probable speed of about $v_0 = 550$ m/s corresponding to a translational temperature of about 75 K. Using both resonantly enhanced two-photon ionization [or resonantly enhanced multiphoton ionization (REMPI) provided anything more than one photon is termed ''multi''] and laser-induced fluorescence, we have established the vibrational temperature of the molecular beam to be about $T_{vib}=150\pm25$ K and a somewhat lower rotational temperature of $T_{rot}=75\pm25$ K. At these values, about 80% of the Na_2 molecules are in the ground vibrational level and 5% excited beyond $v=1$ while the most probable rotational level is found at around $J\approx12$.

The laser system used in the experiments consists of a 20-Hz *Q*-switched Nd:YAG (continuum model NY-61) and two tunable dye lasers (Lumonics Hyper-dye 300). Typical specifications are pulse duration of about 7 ns for the YAG and slightly shorter for the dye lasers, a dye laser band width of approximately 0.1 cm^{-1}, and pulse energies of approximately 10 mJ for the dye laser at 620 nm. In order to minimize multiphoton effects, the dye laser power is reduced in the experiments to about 10 μJ. Because of a relatively long distance, the laser-beam diameter has increased to ca. 10 mm at the intersection with the molecular beam corresponding to a power density level of about 20 kW/cm^2; an aperture at the entrance window of the vacuum chamber limits the laser to a diameter of about 3 mm. A Rochon polarizer cube assures the dissociation laser degree of linear polarization to better than 1 part in 10^5. For the fragment angular distribution measurements, rotation of the probe laser polarization is accomplished with the help of a double Fresnel rhomb. Finally, for the ancillary two-color REMPI experiment used to characterize the internal Na_2 state distribution, frequency doubling with a potassium dihydrogen phosphate crystal, produces the UV light necessary to ionize the $A\,^1\Sigma_u^+$ state excited Na_2 molecules.

Our TOF spectrometer is designed to give optimized space focusing when acceleration and extraction voltages, V_{ac} and V_{ex} are adjusted to a ratio of $V_{ac}:V_{ex}=4$. The residual flight-time spread of Na_2^+ ions starting at the top and bottom of the molecular beam, respectively, is then predicted to be 50 ns for the typical operation value of $V_s=7.5$ V. Other experimental parameters influencing the spread of arrival times of monoenergetic fragments are primarily the finite solid angle of the ion detector, a small amount of ac voltage noise residing on some of the spectrometer electrodes, the residual perpendicular beam velocity components of the Na_2 molecules, and fringe fields produced by the wires of the meshes that separate the various regions of the TOF spectrometer. We discuss these influences in Sec. IV describing the simulation program.

Finally, data acquisition is accomplished by coupling the output of our microchannel plate detector into a 100-MHz

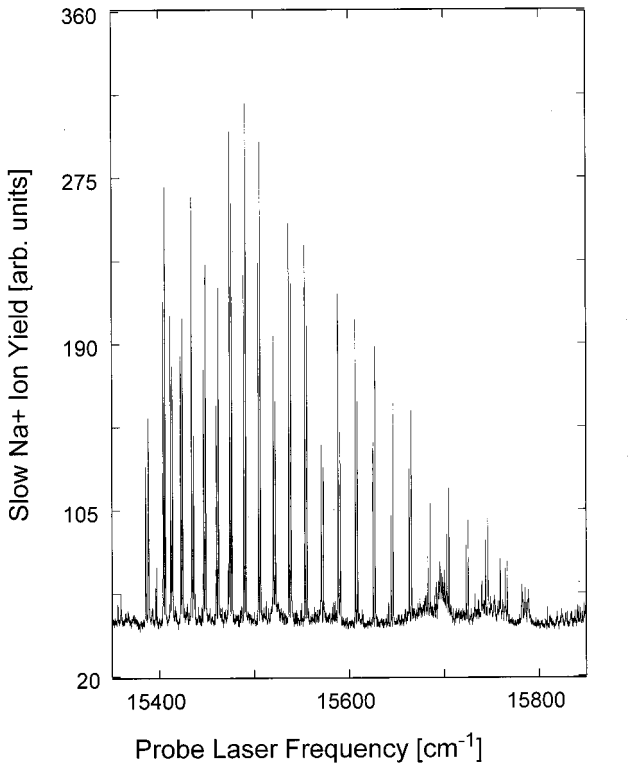

FIG. 2. The Na^+-ion yield spectrum in this figure was obtained by exciting Na_2 molecules to the $v'=20$, $N'=15$ level of the $A\,^1\Sigma_u^+$ state, scanning the probe laser over the indicated range, and collecting slow Na^+ ions with flight time between 26 and 27 μs (see Fig. 3).

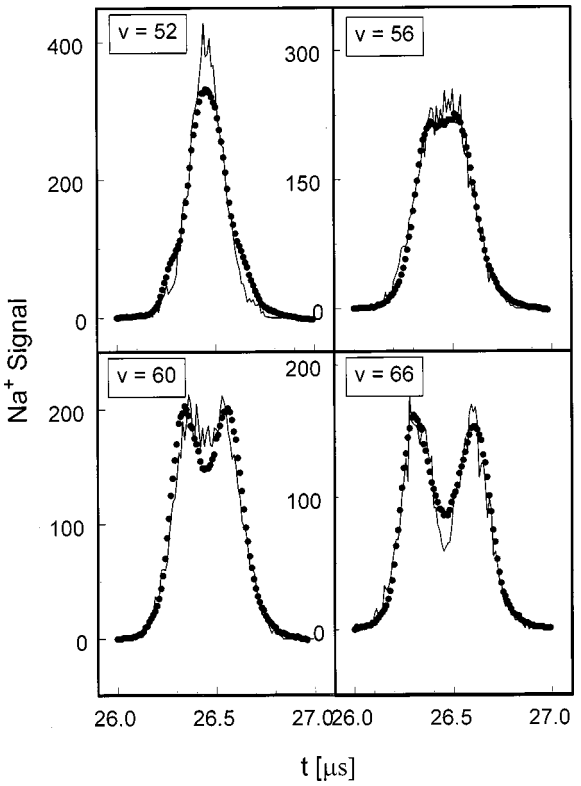

FIG. 3. Experimental time-of-flight spectra (solid circles) of slow Na^+ ions produced in dissociative ionization of Na_2 in rovibrational levels of the 4 $^1\Sigma_g^+$ state as indicated ($v=52$, 56, 60, and 66). The parent molecule rotational level is $J=16$ in each case. The result of a Monte Carlo simulation is also shown (solid line); see text for further details.

transient digitizer or—for the ion yield data—a suitably gated boxcar integrator. All data is stored for further analysis in a desktop computer that is interfaced to the experiment either via GPIB or an input/output card with analog-to-digital conversion capability.

Procedure. The experiments described here are quite involved. Several separate steps have to be taken, even ignoring the various experiments needed to obtain a detailed characterization of our experimental setup, chiefly for the benefit of a realistic Monte Carlo simulation and hence reliable interpretation of the data. First, we record a two-color REMPI spectrum of Na_2^+ ions via the $A\,^1\Sigma_u^+$ state: the fixed frequency probe laser with a wavelength of about 310 nm ionizes this intermediate state as it is populated when the pump laser is scanned through the absorption region around 610 nm. Assignment of the—rotationally resolved—lines in the yield spectrum allows us to determine unambiguously and independent of any other dye laser calibration the dye laser setting that will excite to a particular rovibrational level of the A state (typically we chose the $v_A=20$, $J_A=15$ level that is a compromise between optimizing signal strength and finding well-isolated molecular transitions). Next, after establishing the desired frequency setting of the pump laser, we remove the UV doubling stage from the probe laser, and record the slow Na^+ ion yield spectrum that arises when the probe laser is scanned through the rovibrational resonances of the shelf 4 $^1\Sigma_g^+$ state. Figure 2 gives an example. Finally, we select the probe-laser frequency needed to populate, via double resonance, the various vibrational levels with rotational selection either via P or R branch excitation, and change to the TOF data acquisition mode. Although proper adjustment of the laser powers minimizes any ion signal from either laser alone, an optical delay of about 10 ns of the probe relative to the pump laser simplifies matters further by precluding any pump-laser ionization of excited Na_2 molecules, which might be produced by accidental resonances of the probe laser. Nevertheless, we record TOF spectra for all possible on-off combinations of the two dye lasers and appropriately subtract the background due to any laser alone (usually this amounts to only a few percent of the total signal, if any). In the end, we obtain TOF spectra such as that shown in, e.g., Fig. 3 built up from typically about 5000 laser pulses.

III. RESULTS

Figures 3 and 7 contain examples of TOF spectra we have measured. In all, spectra for 28 different initial quantum states were recorded: P and R branch excitation out of $v_A=20$ and $J_A=15$ into the shelf vibrational levels $v=50$ to 60, 63, 66, and 69. Shown in Fig. 3 are the cases for dissociative ionization out of the shelf vibrational levels $v=52$, 56, 60, and 66 (filled circles in the figure); a spectrum for $v=50$ is given in Fig. 7. In all cases, fragment flight times are confined roughly to a window of ± 0.5 μs centered about the flight time of Na^+ ions that have no velocity component along the TOF axis, which under our conditions has the

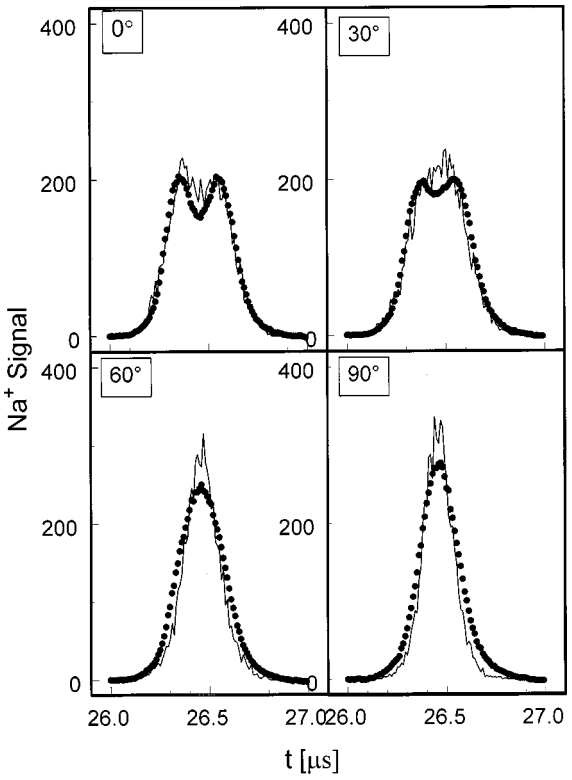

FIG. 4. Polarization dependence of the flight time spectrum of slow Na^+ ions due to dissociative ionization of the $v=60$ shelf vibrational level (solid circles). The angle of the laser polarization with respect to the TOF axis, i.e., the vertical, is shown in each panel. Corresponding Monte Carlo simulations are also included (solid line); see text for further details.

value of 26.47 μs. It is worth emphasizing at this time that because of the double-resonance excitation scheme and the subtraction technique used to generate the shown spectra, there is virtually no contamination due to spurious ionization of atomic Na. Figure 3 shows in particular, for the two highest vibrational levels (60 and 66), the typical forward and backward peaks indicating fragments ejected initially towards and away from the detector. The data shown in the figure should not be interpreted as if the experimental spectra showed monotonically increasing turn-around times for increasing vibrational level (and hence increasing total energy dumped into the molecule). As we reported in our previous note [8], such a simple trend exists only above vibrational level 57 whereas below that level an irregular pattern of peak separation as a function of vibrational quantum number prevails. For the shelf level $v=60$, we have also measured how the TOF spectrum changes when the polarization direction of the probe laser is rotated. Starting at vertical orientation and with a step size of 15°, the polarization angle with respect to the vertical was rotated through 180° and under otherwise identical conditions TOF spectra were recorded. Results for polarization directions of 0°, 30°, 60°, and 90° are displayed in Fig. 4 (again experimental data are represented by full circles). It is interesting to note that despite the parallel nature of the dissociating transition and its associated $\cos^2$ angular fragmentation pattern, the total observed fragment flux at 90° is only by about 10% smaller than that at 0°. Taken literally—and erroneously neglecting the vagaries of detection efficiencies of a TOF spectrometer for slow fragments—the ratio of these two intensities implies an anisotropy parameter of only 0.1 or almost completely isotropic behavior. Obviously, a more refined analysis is necessary and will be presented in the next section.

IV. SIMULATION

The basic ideas and implementation principles of the simulation program used in the analysis of this paper have already been outlined elsewhere [8]. Also, essentially the same code has been described in another paper where it is employed to analyze proton TOF spectra resulting from photodissociation of HBr_n clusters [19]. Generally, the Monte Carlo program propagates the trajectories of a predetermined number of ions through the spectrometer with ion initial positions and velocities chosen randomly but commensurate with appropriate kinetic energy and angular distributions (see below for details). If in the simulation an ion reaches the detector, its flight time is saved and a count in the corresponding time bin is registered contributing to the TOF spectrum thus synthesized.

Fragment energy distribution. The kinetic-energy distribution of the fragment ions was obtained under the assumption that the Born-Oppenheimer approximation is valid. Energy above threshold is shared between the photoelectron, the Na^+ photoion, and the Na($3s$) neutral fragment. The latter two have essentially the same mass and hence evenly split the energy not carried away by the photoelectron. With a total available energy of $E_{\max}$ in the center-of-mass (c.m.) frame, the probability $p(E)dE$ for the heavy fragments to have energy in the range from E to $E+dE$ can then be calculated from

$$p(E)dE = c\sigma(\varepsilon = E_{\max} - E, 1) f(v, J; E, \ell) dE, \qquad (1)$$

where c is an energy-independent normalization constant, $\sigma(\varepsilon, l)$ is the photoionization cross section leading to a free electron with energy ε and angular momentum l, and $f(v, J; E, \ell)$ is the Franck-Condon density for a transition from rovibrational shelf state level $|v, J\rangle$ to a $1\,^2\Sigma_u^+$ scattering state $\langle E, \ell|$ with energy E and orbital angular momentum ℓ. Following the same reasoning discussed at length in our previous paper [8], we have adopted a constant photoionization cross section for the energy range above threshold that we are interested in. Hence, the Franck-Condon density alone is used as a predictor for the slow ion fragment kinetic-energy distribution observed in our experiments. We have numerically evaluated the overlap integrals between the appropriate bound vibrational and free scattering wave functions with the help of a Numerov-Cooley algorithm [20]. For the initial $4\,^1\Sigma_g^+$ state we used a spline-fitted version of the published Rydberg-Klein-Rees potential [21]. For the final $1\,^2\Sigma_u$ Na_2^+ potential $V_u(R)$, written as the sum of polarization and exchange interaction, we have adopted the analytical expression [9]

$$V_u(R) = V_p(R) + V_x(R), \qquad (2)$$

where

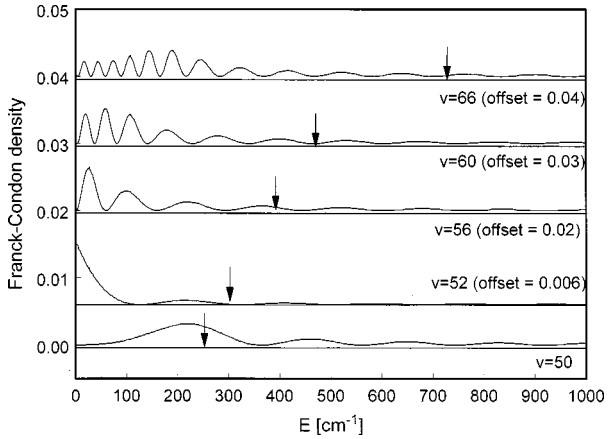

FIG. 5. Franck-Condon densities as a function of fragment energy in the c.m. frame for dissociative ionization of Na_2 in a specific rovibrational level of the 4 $^4\Sigma_g^+$ state; $v=52$, 56, 60, and 66 as indicated.

$$V_p(R)=-\frac{1}{2}\left(\frac{\alpha_1}{R^4}+\frac{\alpha_2}{R^6}+\frac{\alpha_3}{R^8}-\frac{B}{R^7}\right) \tag{2a}$$

and

$$V_x(R)=\frac{1}{2}A^2R^{2/\beta-1}e^{-\beta R-1/\beta}\left[1-\left(\frac{1}{\beta^3}-\frac{1}{\beta^2}\right)\frac{1}{R}\right]^2 \times\left[1+\left(\frac{3}{2\beta^3}-\frac{1}{\beta^2}\right)\frac{1}{R}\right], \tag{2b}$$

which gives excellent fits to earlier published calculations [9–15] of the 1 $^2\Sigma_u^+$ potential. A nonlinear fitting procedure based on the Levenberg-Marquardt algorithm produces best fit parameters for the various potentials, which we have assembled in Table I. Also included in this table are the corresponding zero-energy crossing points R_0 and well depths $V_{\min}$ (note that the fit parameters are given in atomic units while R_0 is in Å and $V_{\min}$ in cm^{-1}). Because some of the *ab initio* calculations employ different values of the asymptotic energy, i.e., of the ionization potential of Na, we have shifted the potential data of these references by the difference between their value and our adopted value [22] of $V_{\rm ion}$ (Na)=41449.65 cm^{-1}=0.188859 a.u.

Because of the double-resonance excitation scheme used in our experiments, the total energy $E_{\max}$ in Eq. (1) is completely determined by very accurately known spectroscopic data. Once the assignment has been made as to which rovibrational levels (v_A,J_A) and (v,J) of the $A\,^1\Sigma_u^+$ and 4 $^1\Sigma_g^+$ states, respectively, are involved in a given TOF spectrum, the total available energy $E_{\max}(v_A,J_A,v,J)$ follows immediately from the relation,

$$E_{\max}(v_A,J_A,v,J)=2E_{4\Sigma}-E_{A\Sigma}-D_e(X\,^1\Sigma_g^+)-V_{\rm ion}({\rm Na}), \tag{3}$$

when the above-quoted value for the ionization energy of the ground-state Na atom is used; $D_e(X\,^1\Sigma_g^+)=6022.0286\,{\rm cm}^{-1}$ for the dissociation energy of the Na_2 ground state [23], and the spectroscopic terms $E_{A\Sigma}$ and $E_{4\Sigma}$ refer to the appropriate term energies of the $A\,^1\Sigma_u^+$ and 4 $^1\Sigma_g^+$ states, respectively [24,21].

Figure 5 exemplifies the behavior of the Franck-Condon density that is sampled by dissociative ionization starting in the shelf vibrational levels indicated in the figure. These are the same levels for which the corresponding flight time spectra are reproduced in this paper. Note the pronounced peak at zero fragment energy for the shelf level 52. Its outer turning point of 9.3 Å [21] is situated perfectly to couple the low momentum part of the bound wave function very effectively into the zero-energy scattering wave function launched at the 1 $^2\Sigma_u^+$ zero-energy crossing point of about 8.8 Å (see Fig. 1). Also indicated in Fig. 4 are the respective total available energy values.

Fragment angular distribution. In accordance with the symmetry of the two potentials involved, the 4 $^1\Sigma_g^+$ state of the neutral precursor and the final 1 $^2\Sigma_u^+$ ion state, we expect a value of $\beta=2$ in the standard anisotropy expression [25] for fragmentation of rotationless molecules. However, the initial rotational motion of the Na_2 ($J=14$ or 16) does affect the angular distribution somewhat. In our first communication [8], we argued that even for slow fragments the molecular axis rotates by only small angles—mainly because the internuclear distance and hence the moment of inertia are very large already at the start of dissociation. Rotational effects are indeed negligible for fragments with kinetic energies above about 200 cm^{-1} (in the c.m. frame), but a small yet noticeable influence on the shape of the simulated TOF spectra can be detected for very slow fragments that after all are important in our results. We have, therefore, incorporated a semiclassical, fragment energy-dependent correction [26] to the anisotropy parameter β as follows:

$$\beta_{\rm eff}=\beta P_2(\cos\theta)=\beta P_2\left\{\cos\left[\tan^{-1}\left(\frac{v_{\rm rot}}{v_{\rm trans}}\right)\right]\right\} \tag{4}$$

with

$$v_{\rm rot}=\frac{\hbar\sqrt{\ell(\ell+1)}}{\mu\langle R\rangle} \tag{4a}$$

and

$$v_{\rm trans}=\sqrt{2E/\mu}, \tag{4b}$$

where in Eq. (4) P_2 denotes the second Legendre polynomial and the fragment rotational and translational speeds in the center-of-mass frame and $v_{\rm rot}$ and $v_{\rm trans}$, respectively, are spelled out in Eqs. (4a) and (4b). There, ℓ quantifies the fragment orbital angular momentum, μ, the fragment reduced mass, and E, the c.m. fragment energy. The average bond length at the moment of absorption of the last photon $\langle R\rangle$ essentially plays the role of the impact parameter in this semiclassical model of photodissociation viewed as half-collision. We derive its value from the centroid approximation [27] as the expression

$$\langle R\rangle=\langle E,\ell|R|v,J\rangle/\langle E,\ell|v,J\rangle, \tag{5}$$

where $|v\rangle$ and $|E\rangle$ are the properly normalized wave functions describing the initial bound vibrational level v and the scattering state at energy E, respectively. Numerical values are obtained by using the appropriate matrix elements (see above) for each potential in the corresponding integrals. In

each instance, this argument defines a unique value for $\langle R \rangle$, which we then use in evaluating the effective anisotropy parameter β_{eff}. For the parameter values in our case, it is smaller than 1.9 when E decreases below about 200 cm^{-1} ($\simeq$0.025 eV). In particular, for those cases where the energy distribution calls for significant numbers of fragments with low energies, this change in the angular distribution shows up in simulated spectra as a subtle but definitely noticeable ''filling in'' of the minimum between the TOF peaks due to early and late fragments if such a minimum exists (see spectra in Figs. 3, 4, and 7). Otherwise, the influence due to parent rotation on the TOF spectral line shape is very weak; in particular, no noticeable broadening of the lines is seen.

The Monte Carlo simulation of our measured TOF spectra combines all above ingredients leaving only an overall scaling factor and a small (at most $\pm$20 ns) flight time shift as adjustable parameters. Usually, and for the cases shown in the figures, we have adopted the approach to scale experiment and simulation by the ratio of their respective areas. The success of this simulation approach may be gauged by the examples included in Figs. 3, 4, and 7. While in Fig. 3 the scaling factors for each vibrational level are different, the same scaling factor is used for all polarization angles in Fig. 4. This figure shows the measured simulated polarization dependence of the dissociative ionization signal originating in shelf vibrational level $v=60$. We have rotated the probe laser polarization angle in steps of 15°—not all results are displayed—from 0° (equivalent to vertical polarization, parallel to TOF axis) to 90° (horizontal polarization, perpendicular to TOF axis). It is interesting to note that the corresponding change in the TOF line shape is somewhat different from the case familiar at higher fragmentation energy. From the discussion of the fragment angular distribution we know that $\beta=2$; hence, we expect the Na^+ fragments to be ejected in a $\cos^2$ distribution, symmetric around the laser polarization direction. Therefore, for vertical polarization (panel 0° in Fig. 4) we expect and observe the typical, symmetric bimodal peak due to the large number of fragments initially leaving approximately upwards (early peak) and downwards (late peak). As the laser polarization is rotated towards the horizontal direction (panel 90° in Fig. 4), the fragment angular distribution rotates with it thus diminishing the fragment flux appearing at the flight time of those peaks—as one would expect. However, the signal near line center—corresponding to fragments with near zero initial velocity along the TOF axis—actually increases. This is a consequence of the finite solid angle of the detector and the high collection efficiency of the TOF spectrometer for these fragments. As mentioned above, for the measurement of the polarization dependence we scaled the simulation only once to the experimental data (at 0° and by area). The same scaling factor is then used for all other polarization angles. As can be seen all trends of the experimental data are well borne out in the simulation.

V. DISCUSSION

The data of this paper have been analyzed with the procedure outlined in Sec. IV above and the solid lines shown in the TOF spectra of Figs. 3, 4, and 7 are the final results of this effort. Considering the paucity of adjustable parameters,

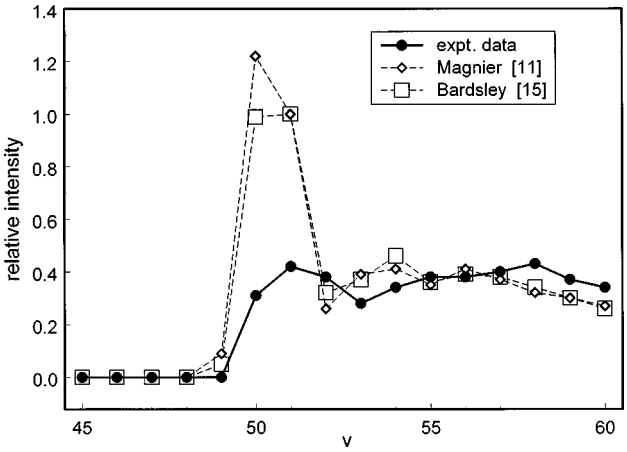

FIG. 6. Relative intensities of slow Na^+ ion yield as a function of shelf vibrational level v. Experimental values are compared with two model calculations (see text for details) involving the potential calculations by Magnier (Ref. [11]) and Bardsley, Junker, and Norcross (Ref. [15]).

the degree of agreement between experiment and simulation is quite satisfactory. In fact, all cases not shown have the same or even better conformity. The underlying potential in all cases is the best fit to the calculated data points by Magnier [11]. However, as is clear from Table I, the results are so close to the other calculations that our data cannot discriminate between them with the exception of Ref. [10]. Using energy distributions derived from the latter potential the simulation produces spectra, specifically for $v=51-54$, which are in much poorer agreement with the experiment than the case shown in this paper. The zero-energy crossing point of this potential is by about 0.4 Å smaller than that of all other calculations (see Table I). Because the local deBroglie wavelength of scattering wave functions in this region is about 1 Å for energies below about 100 cm^{-1}, such a shift of the zero-energy crossing point has a noticeable impact on the overlap with the initial vibrational wave function of the shelf state. More than causing just a subtle change in line shape, the difference in the zero-energy location can be shown to alter the expected relative intensities of the various lines quite drastically. To this end we have evaluated the product of three Franck-Condon factors taken to measure the probability for each of the three transitions involved: $f_1(X,0 \rightarrow A,20)$ for the excitation from the ground state by the pump laser to the $v_A=20$ vibrational level of the A state, $f_2(A,20 \rightarrow 4\Sigma,v)$ for the second resonant step into the vibrational level v of the shelf state, and finally $f_3(4\Sigma,v \rightarrow 1\Sigma_u,E_{\text{max}}) = \int \langle E|v\rangle dE$, the Franck-Condon densities from our simulation summed from threshold $E_{\text{min}}=0$ to the possible limit E_{max} given by Eq. (3). The result of this analysis, arbitrarily normalized at $v=51$, is shown in Fig. 6 together with the experimental results. The latter values are obtained by summing the intensities contained in the TOF spectra such as those shown in Figs. 3, 4, and 7; they are then subsequently scaled to roughly match the calculated intensity prediction in the range above $v=52$. It is quite obvious that major differences exist despite the fact that the crude behavior for the higher vibrational levels is reproduced. The appearance threshold for slow Na^+ from dissociative ionization out of the shelf state is matched reasonably well by the potentials

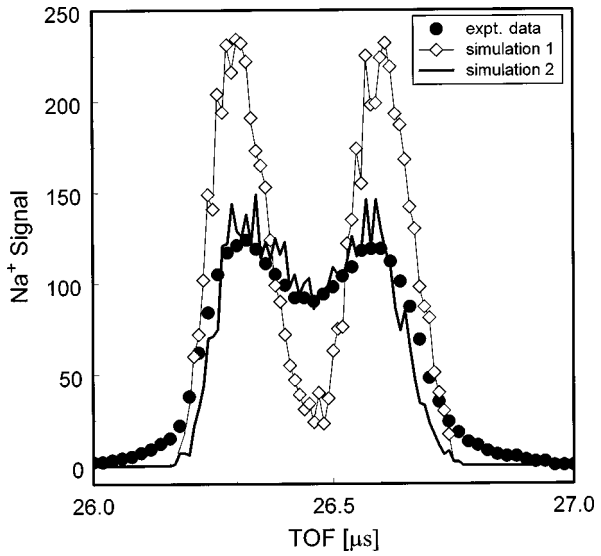

FIG. 7. Experimental time-of-flight spectra of slow Na^+ ions produced in dissociative ionization of Na_2 in a vibrational level 50 of the 4 $^1\Sigma_g^+$ state. The results of two different Monte Carlo simulations are also included differing in the assumed angular distribution of fragments; see text for further details. The better fit is achieved for an isotropic fragment distribution.

used. However, according to this simple model the potential by Tang and co-workers[10]—not shown in Fig. 6 to avoid clutter—would indicate that the unobserved level $v=49$ should exhibit as much intensity as $v=51$ and that $v=50$ would have almost twice this strength (intensity of 2 on the scale of Fig. 6). Likewise, a model potential that we constructed to have a zero-energy crossing point at about 9.3 Å and a well depth of about 70 cm^{-1} yields very small Franck-Condon densities for fragment energies below about 200 cm^{-1} and thus predicts—in contradiction to observation—zero intensity for dissociative ionization out of $v=50$ and a shifting of the appearance threshold to $v=51$. While the potentials used for the simulation of this paper agree with the experiment on the point that the first observed level should be $v=50$ (although the energetic threshold lies at $v=47$), the prediction of a strongly enhanced intensity near the appearance threshold is obviously not borne out by the experiment. Although no particular effort was made during the experiment to keep the probe laser power constant for all TOF spectra, any change was smaller than about 20% and thus should not be sufficient to account for the difference. Also, the assumption of a constant photoionization cross section may not be entirely adequate. On the other hand, it is hard to imagine that for the small energy ranges involved here (see, e.g., Fig. 4) the cross section could change by the factor of almost 3 that is necessary to explain the discrepancy between model and experiment. Possibly a combination of these points and a subtle change in the shape and location of the potential curve could account for the observed discrepancy. In this context, it is interesting to note that although we cannot discriminate between the various potentials—except as mentioned the calculation of Ref. [10]—some of the potentials *do* yield different spectral line shapes for some of the shelf vibrational levels. It is, therefore, tempting to search for ways—among other things, by increased experimental resolution—to extract fragment energy distribution curves in a more direct way from TOF data.

Finally, an exception to the otherwise gratifying agreement between simulation and experiment is the TOF spectrum of dissociatively ionized Na_2 in vibrational level $v=50$ presented in Fig. 7. Because of the $\cos^2$ fragment angular distribution, the fact that the laser polarization is vertical and the fragment energy release very small, the simulation predicts a highly pronounced peak structure (simulation 1 in Fig. 7). Obviously, this is not what the experiment indicates. Better results are obtained when we simulate a TOF spectrum with the same energy distribution, but with an *isotropic* ($\beta=0$) angular distribution (included in Fig. 7 as simulation 2). There is no theoretical reason for this assumption and we will continue to investigate this peculiar behavior.

In summary, we have applied an experimental test to recent calculations of the 1 $^2\Sigma_u^+$ state of the Na_2^+ molecular ion. Monte Carlo simulations of measured flight time spectra of slow Na^+ ions, produced in near-threshold dissociative ionization of quantum state selected Na_2, are consistent with a potential characterized by a zero-energy crossing point at 8.8 Å and a well depth of about 70 cm^{-1}. The zero-energy crossing location in particular, a consequence of the exact balance between exchange and dispersion interaction, seems to be selected by the experiments to within about ± 0.2 Å. Fragment angular distributions have been measured by rotating the polarization direction of the dissociating laser and are compatible with a value of 2 for the anisotropy parameter β as would be expected for the parallel transition involved here. Nevertheless, small corrections to the parameter—caused by the initial parent molecule rotation—are necessary for the best agreement between simulation and data. Two major discrepancies remain: the shape of the vibrational level closest to the observed appearance threshold, $v=50$, cannot be reproduced by the simulation and there is also a much smaller fragment flux near threshold (for $v=50$ and 51) as might be expected from simple Franck-Condon-based arguments.

ACKNOWLEDGMENTS

We gratefully acknowledge the help of Markus Maute and Hong Chen in some of the numerical analyses of this paper.

[1] C. Jungen and S. C. Ross, Phys. Rev. A **55**, R2503 (1997).
[2] P. M. Dehmer and W. A. Chupka, J. Chem. Phys. **65**, 2243 (1976).
[3] H. Rottke and K. H. Welge, J. Chem. Phys. **97**, 908 (1992).
[4] W. T. Hill, B. P. Turner, H. Lefebvre, S. Yang, and J. Zhu, J. Chem. Phys. **92**, 4272 (1990).
[5] M. Ukai, S. Machida, K. Kameta, M. Kitajima, N. Kouchi, Y. Hatano, and K. Ito, Phys. Rev. Lett. **74**, 239 (1995).

[6] S. Yang and W. T. Hill, Phys. Rev. A **51**, 2301 (1995).
[7] E. Charron and A. Suzor-Weiner, J. Chem. Phys. **108**, 3922 (1998).
[8] B. J. Delahunty and L. Hüwel, Phys. Rev. Lett. **80**, 1186 (1998).
[9] C. Johann, S. H. Patil, K. T. Tang, and J. P. Toennies, Chem. Phys. Lett. **295**, 158 (1998).
[10] C. Johann, U. Kleinekathöfer, K. T. Tang, and J. P. Toennies, Chem. Phys. Lett. **257**, 651 (1996).
[11] S. Magnier, Ph.D. dissertation, Université de Paris-Sud, Centre d'Orsay, Orsay, France, 1993.
[12] A. Henriet, J. Phys. B **18**, 3085 (1985).
[13] A. Bähring, I. Hertel, E. Meyer, W. Meyer, N. Spies, and H. Schmidt, J. Phys. B **17**, 2859 (1984).
[14] C. Cerjan, K. Kirby-Docken, and A. Dalgarno, Chem. Phys. Lett. **38**, 401 (1976).
[15] J. Bardsley, B. Junker, and D. Norcross, Chem. Phys. Lett. **37**, 502 (1976).
[16] W. Wiley and I. McLaren, Rev. Sci. Instrum. **26**, 1150 (1955).
[17] B. Delahunty, Ph.D. dissertation, Wesleyan University, Middletown, CT, 1997.
[18] A. Kortyna, D. Reisner, J. Unruh, and L. Hüwel, Phys. Rev. A **50**, 1399 (1994).
[19] R. Baumfalk, U. Buck, C. Frischkorn, N. H. Nahler, and L. Hüwel, J. Chem. Phys. (to be published).
[20] S. E. Koonin, *Computational Physics* (Benjamin-Cummings, Menlo Park, CA, 1986).
[21] C.-C. Tsai, J. Bahns, H. Wang, T.-J. Whang, and W. Stwalley, J. Chem. Phys. **101**, 25 (1994).
[22] C. Moore, *Atomic Energy Levels*, Natl. Bur. Stand. Ref. Data Ser., Natl. Bur. Stand. (U.S.) Circ. No. 35 (U.S. GPO, Washington, DC, 1971), Vol. 467.
[23] K. M. Jones, S. Maleki, S. Bize, P. D. Lett, C. J. Williams, H. Richling, H. Knöckel, E. Tiemann, H. Wang, P. L. Gould, and W. C. Stwalley, Phys. Rev. A **54**, 1006 (1996).
[24] I. Jackowska, W. Jastrzebski, R. Feber, O. Nikolayeva, and P. Kowalczyk, Mol. Phys. **89**, 1719 (1996).
[25] R. Zare, Mol. Photochem. **4**, 1 (1972).
[26] G. Busch and K. Wilson, J. Chem. Phys. **56**, 3638 (1972).
[27] J. Tellinghuisen, in *Advances in Chemical Physics*, edited by I. Prigogine and S. A. Rice (Wiley, New York, 1985), Vol. LX, p. 299.